Experiments in Fluids 23 (1997) 388–394

Mass and momentum transport in longitudinal vortical structures in liquid flow Example of Görtler vortices

P. Petitjeans, J. L. Aider, J. E. Wesfreid

Abstract The difference between mass and momentum transport in longitudinal vortical structures is shown in this paper. The patterns observed by visualization using laser induced fluorescence are the signature of the mass transport, while the flow structures revealed by anemometry show the momentum transport. Experiments and numerical simulations are performed in order to compare the velocity field of the Görtler instability with the mass distribution of a passive scalar. The typical scales involved in this problem are discussed with relation to the Schmidt number, in order to compare the size of the observed "mushrooms" with the size of the longitudinal Görtler vortices. It is found that the nonlinearities which strongly influence the velocity perturbation do not modify the shape and the size of the scalar structures.

1 Introduction

Flow visualization by a passive tracer gives information on mass transport in a flow, whereas velocity measurements, by anemometry for instance, give access to momentum transport. The patterns observed by visualization in liquid are usually quite different from those measured by velocimetry. A careful discussion is needed in order to deduce quantitative information when dye is used as tracer to follow the streamlines, or to display the typical mushroom observed in vortical structures. It has been previously shown that streaklines, pathlines, and streamlines are different in non-steady flows (Hama 1962; Maurel et al. 1996). Even in stationary flows, diffusion, inertia, and topology of the flow can increase the difference between mass and momentum patterns (Simon and Pomeau 1991; Babiano et al. 1994).

In this article, visualizations of flows are obtained with diffusing passive tracers, such as dye in liquid, which is one of the most common ways to visualize a flow. Attention is focused on the complex problem of the difference between the patterns observed in visualization with a diffusing tracer, and the structures existing in the velocity field. Preliminary results have been presented by Petitjeans and Wesfreid (1992), and this problem has been analyzed by Liu and Lee (1990), Finlay et al. (1990), Liu and Sabry (1991), Liu (1991), Liu and Lee (1995). A phenomenological analysis of the typical scales involved in this problem is presented.

This problem is studied both experimentally and numerically in the particular case of spatially developing Görtler vortices. This centrifugal instability appears in boundary layers over a concave wall; the consequence of the imbalance between centrifugal forces and the radial gradient of pressure (Floryan 1991; Saric 1994). Pairs of counter-rotating longitudinal rolls arise in the direction of the main flow (Fig. 1). As with most centrifugal instabilities, nonlinearities have a strong influence on the spatial growth of vortices, long before turbulence appears and at a much smaller Reynolds number than for shear instabilities. In such a three dimensional nonparallel flow, it is difficult to measure the full 3D velocity field in a reasonably large section of flow. This explains why only one or two components of the velocity along some judiciously chosen axes are measured. To determine these axes, visualization is used to get most of the spatial quantities such as wavelength, size of the vortices, and position of their core. This paper shows to what extent visualization can be utilized to interrogate the velocity field, and in what ways it fails.

In order to complement the experimental investigations, a 3-D numerical simulation is performed which gives the full 3-D velocity field and the mass-concentration field. The mass and the momentum transport in the experiment is qualitatively compared with the numerical simulation. For this work, there is no possible quantitative comparison between experiments and simulations, since the initial conditions cannot been matched exactly. Nevertheless, simulations help in the qualitative understanding and interpretation of experiments, and give much information on the spatial evolution of the scalar and velocity fields.

In the first part of this paper, the experimental set-up is presented, as are the methods used to visualize the flow and to obtain the velocity field. In the second part, a comparison between the visualization and the velocity field is discussed, and a phenomenological interpretation of the difference is proposed. The third section explains the numerical method used in the three-dimensional simulation, and the results obtained are described. Finally, an analysis of these results is given which better illuminates the interpretation of visualizations obtained with a diffusive passive tracer.

Received: *19 March 1996*/*Accepted*: *24 March 1997*

P. Petitjeans, J. L. Aider, J. E. Wesfreid
Laboratoire de Physique et de Mécanique des Milieux Hétérogènes
Ecole Supérieure de Physique et de Chimie Industrielles (ESPCI)
10, rue Vauquelin, F-75005 Paris, France

Correspondence to: P. Petitjeans

We acknowledge E. Guyon, J. Liu, H. Peerhossaini, Y. Pomeau, and M. Vartuli for fruitful discussions about this subject. This work was partially supported by SNECMA. Special thanks go to M. Michaelian and R. Bell for their help in proof reading this paper.

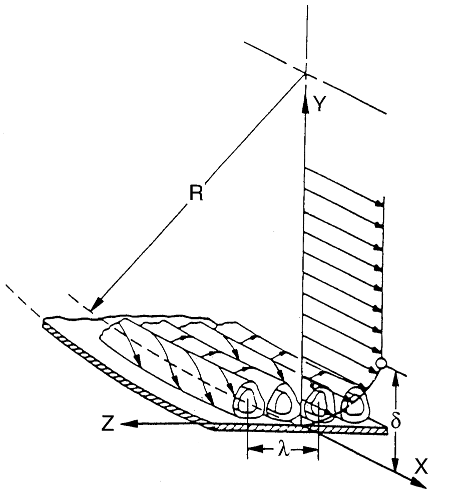

Fig. 1. Görtler vortices in the boundary layer on a concave wall

A key facet of the analysis presented is that it can be partially extended to the problem of thermal transfer using analogy between mass and temperature (in that they are both passive scalars).

2
Experimental set-up and methods

The apparatus is a low velocity water channel specially designed to study the Görtler instability (Peerhossaini and Wesfreid 1988; Petitjeans and Wesfreid 1995; Petitjeans and Wesfreid 1996; Aider and Wesfreid 1996). This set-up is well equipped for Laser Induced Fluorescence visualization, using a light sheet and dye injection facilities. Velocity measurements are obtained through an automatic laser Doppler anemometry (LDA) system. The experimental set-up is shown in Fig. 2.

The flow is generated by gravity with a constant level water tank of capacity 384 liters, located 175 cm above the channel. The flow velocity is controlled with several valves and a flow meter. The channel is built of Plexiglas (1.5 cm thick).
A succession of different sections makes the flow as laminar as possible: a diffuser, a converging section, a diverging section, a settling chamber, a 2D contraction chamber, and a relaxation section where it is possible to inject dye as a sheet or as several jets. The section which follows is the curved section where the Görtler instability is studied. A straight vertical section is attached to the end of the curved section and allows the observation of the persistence of the rolls. The concave test section consists of a curved duct with width, $L_z = 10$ cm (Fig. 2). The radius of curvature of the outer concave wall is $R_o = 10$ cm, and the radius of the inner convex wall is $R_i = 5.7$ cm. The two centers of curvature are slightly different ($d = 0.7$ cm in the horizontal direction) to compensate for the growth of the boundary layers. On each wall, there is a deviation of the flow in the inlet of the curved section to eliminate the boundary layers which are developed upstream.

2.1
Visualization (mass transport)

The structures generated in the curved section are visualized with the Laser Induced Fluorescence method (LIF). The dye is injected far upstream (2 m) without perturbing the flow. The dye current is generated using gravity (from a constant level tank). The difference between the level of dye and the level of water is carefully controlled in order to keep the initial conditions constant and to prevent dye jet instabilities. A light sheet is generated with an argon laser and a cylindrical lens. The dye mixture is a 0.1 g/l concentration solution of Fluoresceine ($C_{20}H_{10}Na_2O_5$) in water, so that the density difference, $\delta\rho/\rho = 10^{-4}$, is negligible. The absorption spectrum

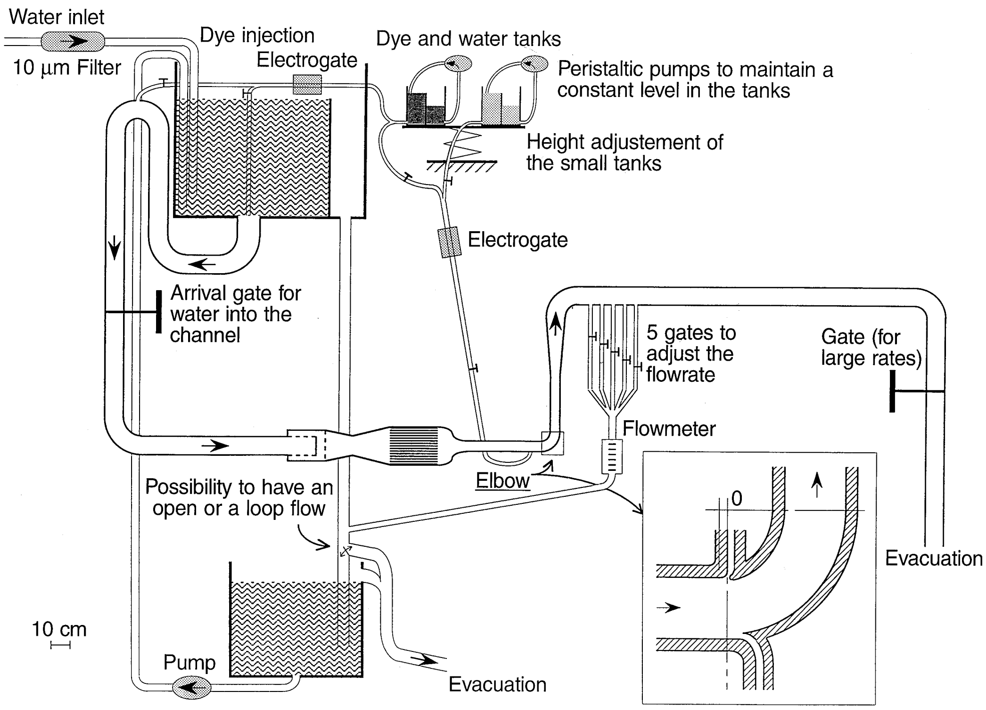

Fig. 2. Experimental set-up

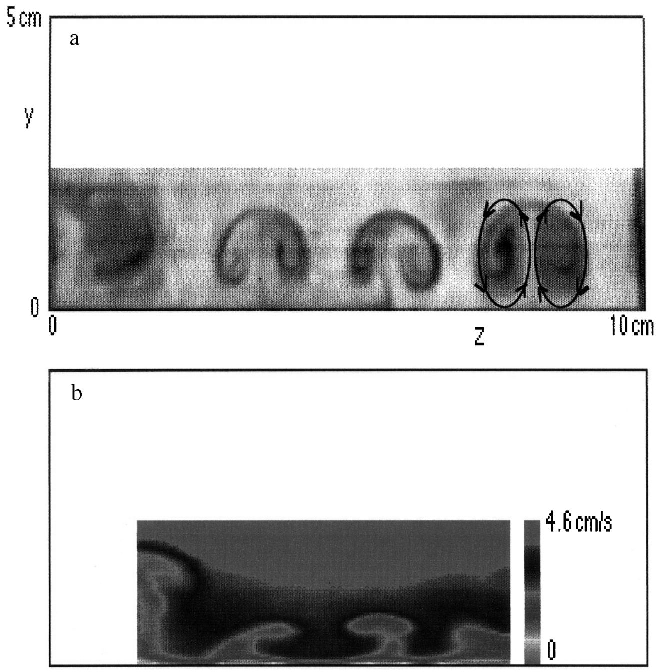

Fig. 3. **a** Visualization in a cross-section, $\alpha = 52°$ from the leading edge. The dark frame represents the walls; **b** streamwise velocity field in the same cross-section as Fig. 3a

is maximum for an excitation wavelength of $\lambda \approx 490$ nm, corresponding to the blue ray of an argon laser light. The light is re-emitted in the green ($\lambda \approx 514$ nm). This method allows observation of structures with vorticity orthogonal to the plane of the light sheet. A cross section of the flow exhibits mushroom-like structures in the boundary layer over the concave wall. Figure 3a is a typical picture obtained with this method in the cross-section $\alpha = 52°$ from the leading edge, in a stationary case with a mean centerline velocity $U_0 = 4.6$ cm/s. This figure also gives a schematic representation of the rolls. The stems of the mushrooms correspond to the region where the rotation of the rolls induces a flow from the concave wall to the external flow, and so increases the local thickness of the boundary layer: this region is called "outflow". In the opposite direction, the region between two mushrooms corresponds to a place where the rotation of the rolls induces a flow from the external flow towards the concave wall, and "crushes" the boundary layer: this region is called "inflow". This representation can be observed in all the centrifugal instabilities, such as the Taylor–Couette instability between two coaxial cylinders in rotation, or the Dean instability in a Poiseuille flow in a curved duct. These structures are also observed in the Coriolis instability in rotating channels which generates longitudinal rolls.

2.2 Velocity field (momentum transport)

The streamwise component of the velocity field is measured with an automatic Laser Doppler Anemometer. This system consists in a fiber optic probe which gives a simple method of positioning the volume which is to be measured in the flow. Titanium Dioxide Particles (TiO_2) are added to the water with a concentration of approximately 0.1 mg/l. Their mean diameter is 50 μm, and their density is close to 1. The streamwise velocity component U is measured to deduce the streamwise perturbation u, because it is the largest perturbation compared to the two other components v and w (as usual for longitudinal vortices). This system is controlled by a computer which records the data. In the same section where a picture is taken of the dye visualization ($\alpha = 52°$), the streamwise stationary velocity field is also "scanned", recording about 2500 velocity measurements (every 0.1 cm in the spanwise direction z, and every 0.05 cm in the radial direction y). In order to compare the two fields (longitudinal velocity and dye concentration), a gray level (between 0 and 255) is associated with each velocity measurement. As a result, a picture is obtained as a representation of the streamwise velocity field (Fig. 3b) where the isochrome lines correspond to iso-velocity lines (streamwise component) in the same cross-section as Fig. 3a, and under the same conditions, because the flow is stationary.

Before making a comparison between mass transport and momentum transport, it is important to note that these measurements allow an observation of the strong influence of the nonlinearities in the velocity field. If the nonlinearities are very weak, the streamwise velocity profile would be sinusoidal in the spanwise direction, z. In that case, the inflow and the outflow regions would have the same spanwise extension. The influence of the rolls in this situation would have no effect on mass transfer (or heat transfer by analogy) between the wall and the external flow: what is taken in the inflow regions (where the gradient of velocity is larger), is exactly compensated by what is lost in the outflow region (where the gradient is smaller). In this experiment (Fig. 3b), this is not the case anymore. Nonlinearities deform the spanwise profile and act such that the inflow regions are much more extended than the outflow regions. The mass (or heat) transfer is largely increased in this type of flow, which is still laminar (Smith and Haj-Hariri 1993). Indeed, these nonlinearities appear very rapidly in the Görtler instability, and in most of flows which produce counter-rotating longitudinal rolls. This asymmetry is more pronounced in the counter-rotating longitudinal rolls than in co-rotating transversal rolls, such as those seen in shear instabilities. Therefore, the production of longitudinal vortices in a laminar flow is a good way to enhance the mass (or heat) transfer without using a turbulent flow. Indeed, the new generation of static high efficiency mixers in heat exchangers or chemical reactors use short longitudinal vortices induced by rows of nuggets to enhance the mixing.

3 Comparison between concentration field and velocity field

In Fig. 3a and 3b, mushrooms are observed which are located in the same spanwise position z. Everything else is different: the size is not the same, neither is the thickness of the patterns.

The Schmidt number is used in order to understand the difference between the thickness of the patterns in these two pictures. The dimensionless Schmidt number, $Sc = \nu / D$, represents the ratio of the vorticity diffusion to the mass diffusion, where ν is the kinematic viscosity, and D is the mass diffusion coefficient. This number can also be written as the ratio of two characteristic times, $Sc = \tau_m / \tau_\nu$, where τ_m is the characteristic time of mass diffusion, and τ_v is the characteristic time of vorticity diffusion. For water and a solution of fluoresceine, $\nu = 1.14 \times 10^{-2}$ cm^2/s and $D = 3.6 \times 10^{-6}$ cm^2/s, corresponding to a Schmidt number $Sc \approx 3200$. Thus mass diffuses about 3200 times more slowly than vorticity. The difference in thickness between the two mushrooms patterns in Fig. 3a and b is given by the ratio of characteristic length of vorticity diffusion ($\delta_v = \sqrt{\nu \tau_v}$) to the characteristic length of mass diffusion $\delta_m = \sqrt{D\tau_m}$, i.e. $\delta_v/\delta_m = \sqrt{\nu/D} = \sqrt{Sc} \approx 56$. Hence, the region between the vortices shown as the stem in the velocity field is wider than that observed in the concentration field, which is compatible with what is observed in Fig. 3.

For gas, the Schmidt number is of order unity, $Sc \approx 1$. In other words, vorticity and mass diffuse the same distance in the same time. Indeed visualization with smoke in gas (Fig. 4b from Ligrani and Niver, 1988) yields similar images to the velocity field shown in Fig. 3b. Similar observations were found in numerical simulations by Liu et al. (same ref. already cited) and Finlay et al. (1990).

This problem of mass diffusion is exactly analogous to the problem of thermal diffusion if temperature can be considered a passive scalar, i.e. if there is no convection induced by the temperature gradient. In this case, the Schmidt number is replaced by the Prandtl number, $Pr = \nu/K$, which represents the ratio of vorticity diffusion effects to thermal diffusion effects.

In order to better understand the difference in size between the mass mushrooms and vorticity mushrooms, the former is compared with the perturbation velocity field. Figure 5 gives measurements of the streamwise perturbation u, and estimations of the radial and spanwise eigenfunctions for the

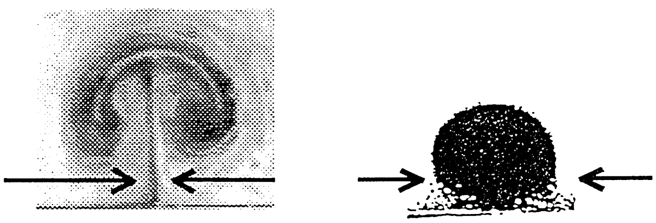

Fig. 4. **a** Visualization in liquid (water); **b** visualization in gas (air) from Ligrani and Niver (1988)

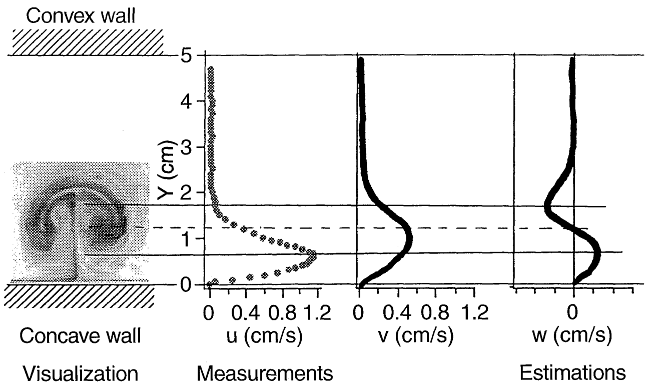

Fig. 5. Interpretation of visualizations

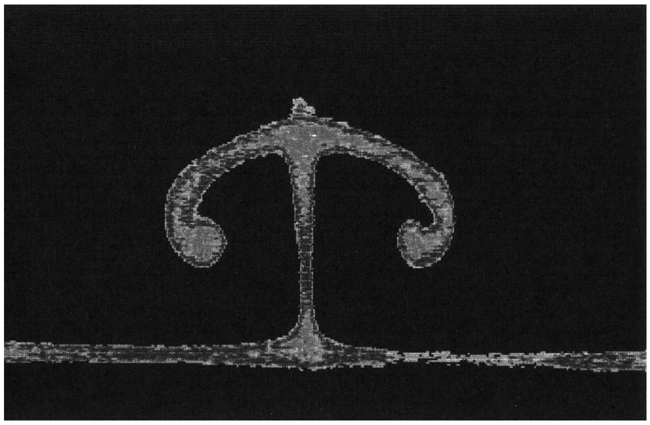

Fig. 6. Pseudo-image showing the concentration of dye. The highest concentration is in the lightest color

perturbations v and w. These estimations are purely qualitative. They are obtained by matching the form of the eigenvalues of Floryan and Saric (1982) and the measurement of u, as well as from the numerical simulations presented later. The maximum radial perturbation is at $y(v_{max}) \approx 0.9$ cm from the concave wall in this experiment. The stem of the mushroom is thinner at this position where the radial velocity, v, is the highest. This is confirmed by Fig. 6, which represents a pseudo-image of a visualization showing the concentration of dye. Indeed, the stem is thinner around the middle ($y \approx 0.9$ cm). This is because the radial velocity, V, is larger in this region. Therefore the dye has less time to diffuse.

The spanwise perturbation w is equal to zero at about the same position where v is maximized. This is the position of the centers of the rolls. In addition, the positions where w is maximized are also obtained ($y \approx 0.3$ cm and $y \approx 1.4$ cm). The location of the center of the Görtler rolls can be deduced and superimposed with the visualization (Fig. 5). The centers of the rolls are located at the extremities of the "hat" of the mushrooms.

4
Numerical simulation

4.1
Numerical method

A fully three-dimensional numerical simulation of steady spatially developing Görtler vortices in a rectangular curved channel is performed. Moreover it is necessary to include a diffusive passive scalar in this simulation with the characteristics of the water-fluoresceine mixture that was used in the experiments. Because of the difficulty in matching the initial conditions with those of the experiments, the simulation will be compared with the experiments only qualitatively.

The Fluent Computational Fluid Dynamics package[1] is used. It is based on a control volume, finite difference method. The numerical method consists of first dividing the domain into discrete control volumes before integrating the differential equations about each individual control volume. The algebraic

[1]from Fluent Inc.

equations are discretized using a curvilinear coordinate system to enable the computation of the flow in complex geometry.

As a passive scalar is simulated in a secondary flow, five basic equations for the convective incompressible fluid have to be solved:

– the mass conservation equation or continuity equation:

$$\frac{\partial \rho}{\partial t}+\nabla\cdot(\rho V)=0 \tag{1}$$

– the momentum conservation equation in three dimensions:

$$\frac{\partial V}{\partial t}+(V\cdot\nabla)V=-\nabla P+\nu\Delta V \tag{2}$$

– and one specie convection-diffusion equation for the passive scalar:

$$\frac{\partial m}{\partial t}+(V\cdot\nabla)m=D\Delta m \tag{3}$$

where m is the mass fraction and D is the diffusion coefficient.

Equations are solved using the SIMPLEC (Semi Implicit Method for Pressure Linked Equation – Consistent) algorithm with an iterative line-by-line matrix solver. The SIMPLEC algorithms are based on using a relationship between velocity and pressure corrections in order to recast the continuity equation in terms of a pressure correction calculation.

As the code does not solve the equations at all points simultaneously, and the equations are coupled and nonlinear, an iterative procedure is required with iterations continuing until all equations are satisfied at all points.

4.2 Geometry and physical properties

The geometry of interest is a 90° curved channel with a 10 cm radius corresponding to the experimental apparatus as illustrated on Fig. 2. To describe completely the flow with good spatial resolution and without increasing the number of cells, the symmetry of the problem is taken into account. A plane of symmetry is imposed as a boundary condition in the middle of the channel. To make sure the Görtler instability is observed (boundary layer instability) and not the Dean instability (Poiseuille flow instability), a constant longitudinal velocity (plug profile) is imposed at the inlet of the duct. The mean streamwise velocity $U_0=4.6$ cm/s corresponds to the experiment, i.e. the boundary layer starts at the edge of the concave plate. The secondary flow is triggered by a small wall perturbator placed just at the beginning of the concave plate. The perturbation is stationary at a fixed position so that the mesh is refined in the region where the vortex will grow. The resolution used in each cross-section plane is 51 nodes in the z direction and 61 in the y direction, with a refined mesh around the vortices. We take 31 planes in the longitudinal direction corresponding to nearly one plane every 3° in the concave part. The dye is modeled as a second non-reactive specie with the same physical characteristics as water, but with a binary diffusion coefficient $D=3.6\times10^{-6}$ cm^2/s corresponding to a Schmidt number $Sc=3200$. It is injected as a 1 mm thick sheet across the span of the inlet, just above the concave wall.

4.3 Numerical results

The spatial evolution of the mass-vortices along the concave plate is illustrated first. Fig. 7 shows the concentration field for eight different longitudinal positions from $\alpha=0°$ to $\alpha=90°$. The dye pattern evolves from a small bump at the beginning of the channel, to a stem 20° downstream, and finally to a "mushroom" like structure at the exit of the channel.

Figure 8 shows the iso-concentration lines (Fig. 8a) and the iso-streamwise velocity lines (Fig. 8b) at the exit of the curved section. This is equivalent qualitatively to what was observed in the experiment (Fig. 3). The thickness of the momentum boundary layer is much larger than the thickness of the mass boundary layer. Again, this confirms that what one can see by visualization in liquid is not necessarily the velocity field.

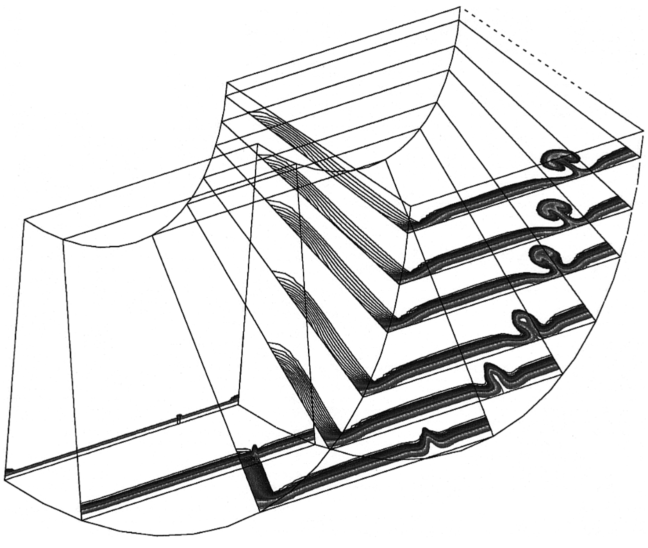

Fig. 7. Concentration fields for eight different longitudinal positions from $\alpha=0°$ to $\alpha=90°$

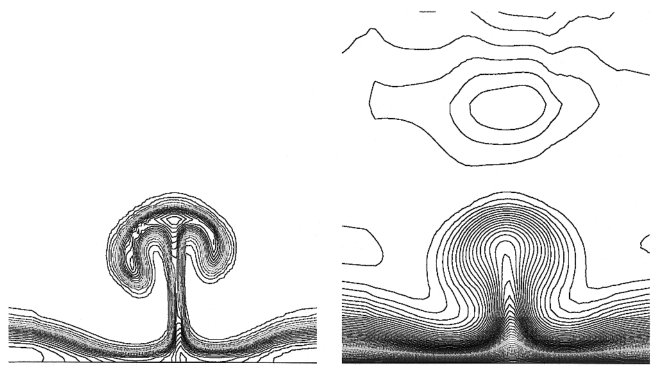

a b

Fig. 8. Iso-concentration lines **a** and iso-longitudinal-velocity lines **b** picture for $\alpha=85°$. The values of the concentration and the velocities for this figure can be obtained from Figs. 11 and 12

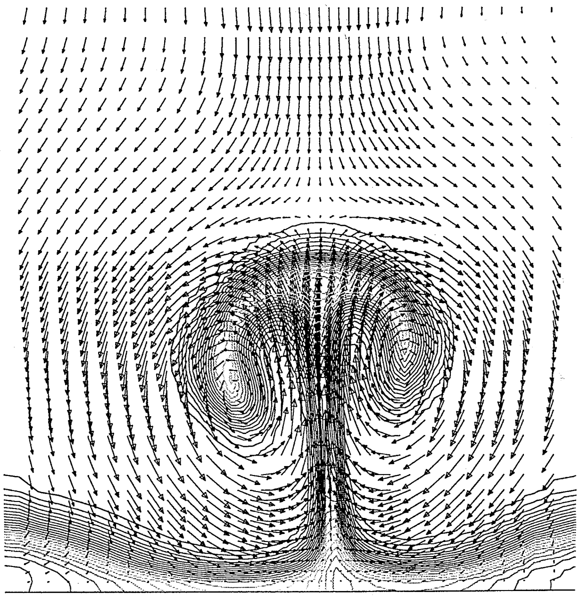

Fig. 9. Iso-concentration lines and transverse velocity field on the same picture for $\alpha = 85^\circ$. The centers of the rolls are near the extremities of the "hat" of the mushroom. The values of the concentration and the velocities for this figure can be obtained from Figs. 11 and 12

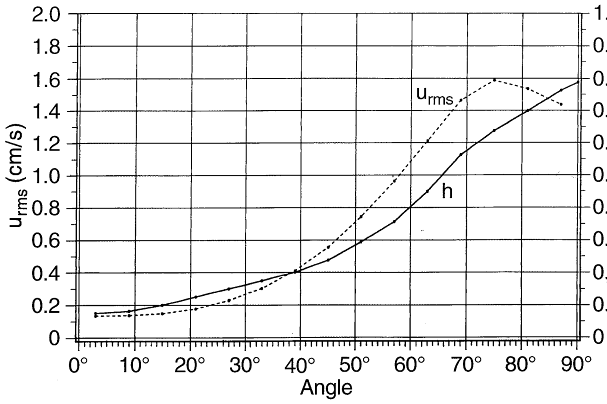

Fig. 10. Spatial evolution of the amplitude of the instability represented by the root mean square of the longitudinal velocity perturbation, and height of the mass-mushroom

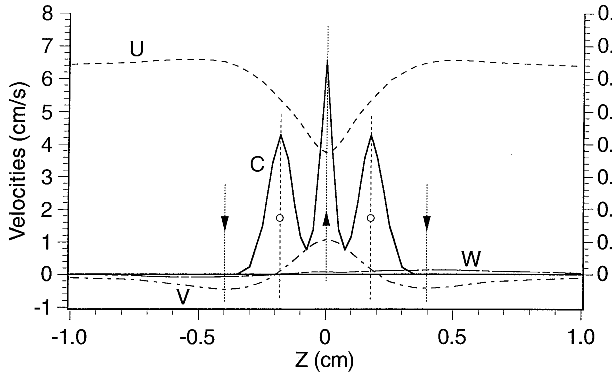

Fig. 11. Velocities and concentration profiles as a function of the spanwise component z at a distance $y = 0.45$ cm from the concave wall and for $\alpha = 85^\circ$. The concentration is scaled between 0 and 1 where $C = 1$ represent the initial concentration of the injected dye

Fig. 9 shows the concentration and the transverse velocity fields on the same picture. This picture shows the real positions of the centers of the rolls which are near the extremities of the "hat" of the mushroom and not between the extremities of the hat and the stem. It is also observed that the lines of iso-transverse velocity, $(v^2 + w^2)^{1/2}$, cross the hat of the mushroom, which is not obvious when observing a visualization. Indeed, one of the most common misinterpretations of such visualizations is to consider that the transverse velocity is tangent to the hat of the mushroom. In reality, this velocity crossing the hat is just the evidence that the vortices still grow in size. In consequence the height of the "mass-mushroom" is not an order-parameter for the instability.

This point is important since many authors have considered the height of the mushroom observed by visualization as a parameter proportional to the amplitude of the perturbation. It is important to understand that this parameter is not relevant. In the case of the Görtler instability, one of the relevant parameters which represent the spatial evolution of the instability is the root mean square of the longitudinal perturbation u, with u such that $U = U_0 + u$, where U_0 is the unperturbed streamwise velocity (Petitjeans and Wesfreid 1995, 1996). Figure 10 shows this parameter u_{rms} as a function of the angle (0° at the entry of the curved section and 90° at the exit). The amplitude of the instability grows until 75° and then decreases because of the nonlinear saturation. On the same graph is represented the height h of the mass-mushroom defined as the position y where the concentration is maximum on its head. The mass-mushroom continues to grow while the amplitude of the instability decreases. Note that h can also be defined as the height, y, at which the concentration drops to 1%, but that does not change the result. This clearly shows that not only the general form of the mass-pattern and momentum-pattern differ, but also that their respective spatial evolutions differ. Plotting v_{rms} or w_{rms} would have given the same streamwise saturation position.

Figure 11 gives on the same graph the velocities U, V, W and the concentration C as function of the spanwise component z at a distance $y^* = 0.45$ cm from the concave wall. $W \approx 0$ at this position y^* means that this position corresponds to the centers of the rolls. The central maximum of dye concentration corresponds to the stem of the mass-mushroom where the radial velocity V is maximum. The two other maxima are at the intersection with the "hat" of the mushroom. The Z location of these two maxima correspond to the positions where the radial velocity V changes sign, i.e. where the centers of the rolls are located. The "valley" in the streamwise velocity, U, is induced by the rolls which lift low speed fluid from the concave wall to the external flow. The width of this "valley" is much wider than any of the concentration peaks since vorticity has diffused much more than concentration.

Figure 12 shows the velocities U, V, W, and the concentration C as a function of the distance y from the concave wall along the stem of the mushroom. We can observe that there are two concentration maxima; one at the upper part of the mushroom, and the second at the lower part near the wall. The concentration maximum near the wall is reminiscent of

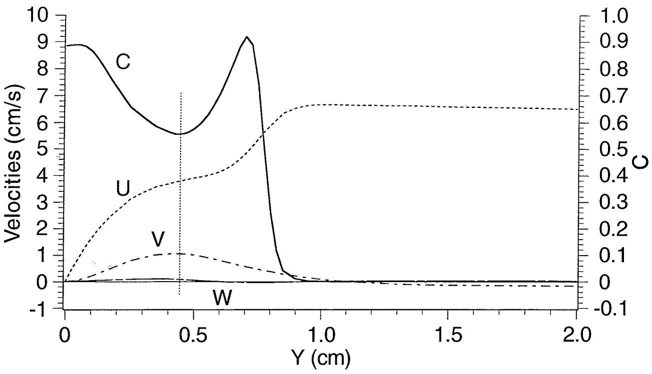

Fig. 12. Velocity and concentration profiles as a function of the distance *y* from the concave wall along the stem of the mushroom and for $\alpha = 85°$

a cellular flow, such as Rayleigh–Bénard convection-cells, that have been seeded with very small particles. The particles accumulate near the wall just below the "ascendant stem", i.e. where the flow is from the bottom towards the top. It is not clear that these two behaviors have the same origin, but it is interesting to note the similarities. Indeed, particles accumulate at this position because of the combination of a stagnation point, gravity, and molecular diffusion (Simon and Pomeau, 1991). In our case, the density difference is very small but not zero ($\delta\rho/\rho = 10^{-4}$), and gravity is not always aligned with the stem of the mushroom due to the curvature of the wall.

The other concentration maximum is located in the head of the mushroom, at the other stagnation point. In these two regions the transverse velocity is very small, and dye has had time to diffuse, i.e. to jump from one streamline to another.

The minimum concentration is at $y^* \approx 0.45$ cm which corresponds to the position where the radial velocity V is maximum, confirming what is observed in the experiment (Figs. 5, 6). In addition, this position y^* corresponds to the height where the centers of the rolls are located (Fig. 11).

5
Conclusion

A phenomenological analysis of the difference between the velocity field and the concentration field has been proposed in the particular case of the Görtler instability from experiments and numerical simulations. Mass and momentum transport have indeed very different properties, particularly in liquids where the Schmidt number is much larger than unity. This implies different patterns sizes and shapes depending on what we measure, velocity or concentration. Also, the centers of the rolls have been located at the extremities of the hat of the mass-mushroom and not between the hat and the stem as would be deduced from a too simplistic analysis of the concentration field.

An important aspect pointed out in this paper is the non-relevance of the height of the mass-mushroom as an indicator for the amplitude of the instability, since it has been observed that the height still increases as the amplitude of the instability decreases under the nonlinear saturation.

This study can be applied to other instabilities where similar structures appear (Floryan and Saric 1982) and also to the case of heat transfer when the temperature can be considered as a passive scalar. This last case is of great interest since many new heat-exchangers are based on the mixing properties induced by longitudinal rolls (created by curvature of vortex generators).

An extension of this work can be done by the analysis of residence time curve (RTC) of mass or temperature pulses introduced at the inlet and observed at the exit of the experimental apparatus. Analysis of these RTC profiles can be used to evaluate the effective molecular diffusion (dispersion) and the degree of normal (gaussian) mixing. This information can be correlated to the pattern of the tracer mushroom (Piva et al. 1996; Castelain 1995).

References

Aider JL; Wesfreid JE (1996) Characterization of longitudinal Görtler vortices in a curved channel using ultrasonic velocimetry and visualizations. J Phys III, 6: 893–906

Babiano A; Provenzale A; Vulpiani A (1994) Chaotic advection tracer dynamics and turbulent dispersion, North-Holland, Amsterdam

Castelin C (1995) Etude expérimentale de la dynamique des fluides et des transferts thermiques dans un écoulement de Dean alterné en régime d'advection chaotique, PhD thesis, ISITEM, Nantes

Finlay WH; Guo Y; Olsen D (1993) Inferring secondary flows smoke or dye flow visualization: two case studies. Phys Fluids A 5: 2689–2701

Floryan JM (1991) On the Görtler instability of boundary layers. Prog Aerospace Sci 28: 235–271

Floryan JM; Saric WS (1982) Stability of Görtler vortices in boundary layers. AIAA J 20: 316–324

Hama FR (1962) Streaklines in a perturbed shear flow. Phys of Fluids 5: 644–650

Le Guer Y; Peerhossaini H (1991) Order breaking in Dean flow. Phys Fluids A 3: 1029–1032

Ligrani PM; Niver RD (1988) Flow visualization of Dean vortices in a curved channel with 40 to 1 aspect ratio. Phys Fluids A 31: 3605–3617

Liu JTC (1991) On scalar transport in nonlinearly developping Görtler vortex flow. Geophys Astrophys Fluid Dynamics 58: 133–145

Liu JTC; Lee V (1990) Advected scalars in a nonlinear, spatially developing Görtler vortices. Bull Am Phys Soc 35: 2230

Liu JTC; Lee K (1995) Heat transfer in a strongly nonlinear spatially developing longitudinal vorticity system. Phys Fluids A 7: 559–599

Liu JTC; Sabry AS (1991) Concentration and heat transfer in nonlinear Görtler vortex flow and the analogy with longitudinal momentum transfer. Proc Royal Soc A 432: 1–12

Maurel A; Ern P; Zielinska BJA; Wesfreid JE (1996) Experimental study of self-sustained oscillations in a confined jet. Phys Rev E 54: 3643–3651

Peerhossaini H; Wesfreid JE (1988) On the inner structure of streamwise Görtler rolls. Int J Heat Fluid Flow 9: 12–18

Petitjeans P; Wesfreid JE (1992) Structure and perturbation in Görtler vortex flow. In: "Ordered and turbulent patterns in Taylor-Couette flow" (eds. D. Andereck, F. Hayot) Publ. Press, pp 245–251

Petitjeans P; Wesfreid JE (1995) Effect of curvature on the velocity profile and boundary layer in flow through a curved channel. La Recherche Aerospatiale 2: 125–138

Petitjeans P; Wesfreid JE (1996) Spatial evolution of Görtler instability in a curved duct of high curvature. AIAA J 34: 1793–1800

Piva M; Calvo A; Aguirre A; Callegari G; Gabbanelli S; Rosen M; Wesfreid JE (1997) Hydrodynamical dispersion in propagative Taylor–Couette cells. Jour. de Physique III, 7: 895–908

Saric WS (1994) Görtler vortices. Ann Rev Fluid Mech 26: 379–409

Simon B; Pomeau Y (1991) Free and guided convection in evaporating layers of aqueous solutions of sucrose. Transport and sedimentation of solid particles. Phys Fluids A 3: 380–384

Smith ST; Haj-Hariri H (1993) Görtler vortices and heat transfer: a weakly nonlinear analysis. Phys Fluids A 5: 2815–2825